© 2017. Published by The Company of Biologists Ltd | Development (2017) 144, 2798-2809 doi:10.1242/dev.153528

RESEARCH ARTICLE

Wnt signalling controls the response to mechanical loading during zebrafish joint development

Lucy H. Brunt[1], Katie Begg[1], Erika Kague[1], Stephen Cross[2] and Chrissy L. Hammond[1,*]

ABSTRACT

Joint morphogenesis requires mechanical activity during development. Loss of mechanical strain causes abnormal joint development, which can impact long-term joint health. Although cell orientation and proliferation are known to shape the joint, dynamic imaging of developing joints *in vivo* has not been possible in other species. Using genetic labelling techniques in zebrafish we were able, for the first time, to dynamically track cell behaviours in intact moving joints. We identify that proliferation and migration, which contribute to joint morphogenesis, are mechanically controlled and are significantly reduced in immobilised larvae. By comparison with strain maps of the developing skeleton, we identify canonical Wnt signalling as a candidate for transducing mechanical forces into joint cell behaviours. We show that, in the jaw, Wnt signalling is reduced specifically in regions of high strain in response to loss of muscle activity. By pharmacological manipulation of canonical Wnt signalling, we demonstrate that Wnt acts downstream of mechanical activity and is required for joint patterning and chondrocyte maturation. Wnt16, which is also downstream of muscle activity, controls proliferation and migration, but plays no role in chondrocyte intercalation.

KEY WORDS: Joint, Mechanics, Wnt, Morphogenesis, Zebrafish, Cartilage

INTRODUCTION

The developing skeleton is subject to many biomechanical forces, including those from foetal/early postnatal muscle activity. It has become clear from studies on animal models that mechanical stimuli are required for accurate functional joint formation (Nowlan et al., 2010b; Rolfe et al., 2013). For example, *Pax3*$^{sp/sp}$ (*splotch*) mutant mice, which lack limb muscle, and *Myf5*$^{-/-}$*Myod*$^{-/-}$ double mutants, which lack all muscle, show altered morphology in many joints, including elbows and shoulders (Gomez et al., 2007; Kahn et al., 2009; Nowlan et al., 2010a; Rot-Nikcevic et al., 2006, 2007). In chick, paralysis or removal of muscle through grafts results in a knee joint that lacks refinement (Murray and Selby, 1930; Roddy et al., 2009). Zebrafish mutants that lack neuromuscular nicotinic receptors (*nic* b107 mutants) and are therefore immobile, display jaw morphology abnormalities, such as smaller and wider elements (Shwartz et al., 2012). Zebrafish jaw joint morphology is also affected by paralysis, particularly in regions associated with high compressive strain (Brunt et al., 2015, 2016b). In humans, a biomechanical stimulus *in utero* and in newborns has a long-term impact on skeletal health (reviewed by Shea et al., 2015). For example, foetal akinesia deformation sequence (FADS) can cause arthrogryposis owing to reduced foetal movement (Nayak et al., 2014). Risk factors such as breech birth (Luterkort et al., 1986) and swaddling that restrict hip joint movement (Clarke, 2014) can cause developmental dysplasia of the hip (DDH) (Sugano et al., 1998). If left untreated, the abnormal joint shape in DDH can lead to early onset osteoarthritis (OA) (Mavčič et al., 2008). Thus, diverse vertebrate species ranging from fish to humans rely on muscle activity to provide mechanical stimuli to activate the cellular processes required to shape joints during development. This process also has an impact on joint function and health later in life.

Mechanical stimulus can activate genes that are important for skeletogenesis. *In vitro* experiments have shown that application of force to chondrocytes can lead to activation of genes, including those encoding cartilage matrix proteins, such as Type II collagen and aggrecan, and proteins involved in GAG synthesis (reviewed by Grad et al., 2011). Biomechanical stimuli have been widely documented to regulate signalling genes involved in skeleton formation *in vivo*, including constituents of the BMP and Wnt pathways and *Ihh* (reviewed by Chen et al., 2010; Nowlan et al., 2008). In order for mechanical activity to shape the skeleton, alterations to cell behaviour need to occur. A reduction in cell proliferation has been reported in regions of the joint affected morphologically by immobilisation, such as the intercondylar fossa in chick knee joints, mouse mandibular condyles and the joint interzone of *splotch* mice (Jahan et al., 2014; Kahn et al., 2009; Roddy et al., 2011). Cell orientation changes are seen in the jaw cartilages of zebrafish that lack muscle activity (Brunt et al., 2015; Shwartz et al., 2012). Mechanical stimuli are also required for tendon and ligament formation and maturation in species ranging from zebrafish to humans (Chen and Galloway, 2014; reviewed by Chen and Galloway, 2017). Although cell proliferation and orientation at joints have been shown to be biomechanically controlled, as yet, the signals and pathways that transduce the mechanical stimuli into a cellular response have not been fully elucidated.

Wnts are a family of secreted signalling glycoprotein molecules that play vital roles in development, health and disease (reviewed by Niehrs, 2012). Classically, Wnt ligands were subdivided into those that activate the canonical β-catenin pathway or the non-canonical pathways such as planar cell polarity (PCP) and calcium-mediated pathways. However, a more recent consensus is that control of the pathway is interlinked and that Wnt ligands can activate multiple pathways depending on tissue type and cellular context (Willert and Nusse, 2012). Many Wnts, including Wnt4, Wnt5b and Wnt9a (which typically operate in the canonical pathway), and non-

[1]Physiology, Pharmacology and Neuroscience, University of Bristol, Bristol BS8 1TD, UK. [2]Wolfson Bioimaging Facility, University of Bristol, Bristol BS8 1TD, UK.

*Author for correspondence (chrissy.hammond@bristol.ac.uk)

C.L.H., 0000-0002-4935-6724

Received 19 April 2017; Accepted 14 June 2017

Development (2017) 144, 2798-2809 doi:10.1242/dev.153528

canonical Wnt5a are expressed in developing skeletal elements and are implicated in roles such as regulation of chondrocyte differentiation (Church et al., 2002; Hartmann and Tabin, 2000; Yang et al., 2003) and of joint cell identity (Guo et al., 2004; Hartmann and Tabin, 2001). Wnt4, Wnt16, Wnt11 and sFRP2 are all expressed at developing joints (Guo et al., 2004; Ikegawa et al., 2008; Pazin et al., 2012; Rolfe et al., 2014; Witte et al., 2009). Members of the Wnt signalling pathway have also been identified as mechanosensitive. For example, dynamic loading of cultured mesenchymal stem cells affects the regulation of Wnt-related genes such as *Fzd7*, *Wnt3*, *Wnt5a* and *Wnt8* (Arnsdorf et al., 2009; Haudenschild et al., 2009). A decrease in canonical β-catenin reporter construct activation was found in 'muscleless' *splotch* mouse mutants at the joint (Kahn et al., 2009). A transcriptomic study comparing gene expression changes in humerus tissue between control and *splotch* mouse mutants demonstrated that loss of limb muscle led to dysregulation of 34 members of the Wnt signalling pathway – more genes than in any other signalling pathway (Rolfe et al., 2014). These included Wnt ligands, Wnt modulators and Wnt downstream targets. Therefore, Wnt signalling activity in skeletal tissue is mechanosensitive and a candidate pathway for acting downstream of mechanical stimuli in skeletogenesis.

Here, we describe cell behaviours that contribute to changes in joint morphology by following live zebrafish joint development under normal or reduced biomechanical conditions. We demonstrate that canonical Wnt activity transduces mechanical signalling to bring about cell behaviours such as proliferation, migration, intercalation and cell morphology changes that are required to shape the joint. We show that Wnt16 controls cell proliferation and migration specifically in cells at the jaw joint of the lower jaw.

RESULTS

Canonical Wnt signalling is active at regions of high strain in the zebrafish lower jaw

Finite element (FE) models, which map the location of strains acting on the zebrafish lower jaw during mouth opening and closure (Brunt et al., 2015), were used to identify signalling activity in areas of high strain. High levels of tensile (Fig. 1A) and compressive (Fig. 1A′) strains from mouth-opening muscles are exerted at the anterior of Meckel's cartilage (MC) and at the outer region of the jaw joint. During mouth closure muscle activity, high strain is present across the jaw joint interzone (Fig. 1B,B′). The canonical Wnt reporter line *Tg(7xTCF.XlaSiam:nlsGFP)* (Moro et al., 2012) reveals that cells responding to Wnt are located surrounding the lower jaw at 5 days post fertilisation (dpf) (Fig. 1A″), with a population of GFP-positive (GFP+) cells of different morphologies surrounding the anterior Meckel's cartilage (MC) and the jaw joints (Fig. 1A″,B″). This localisation of GFP-positive cells is enriched in regions of the jaw that experience high strain, such as the joint and the symphysis of Meckel's cartilage.

We therefore studied jaw expression of the Wnt reporter from 3-5 dpf, a time previously identified as being crucial for joint

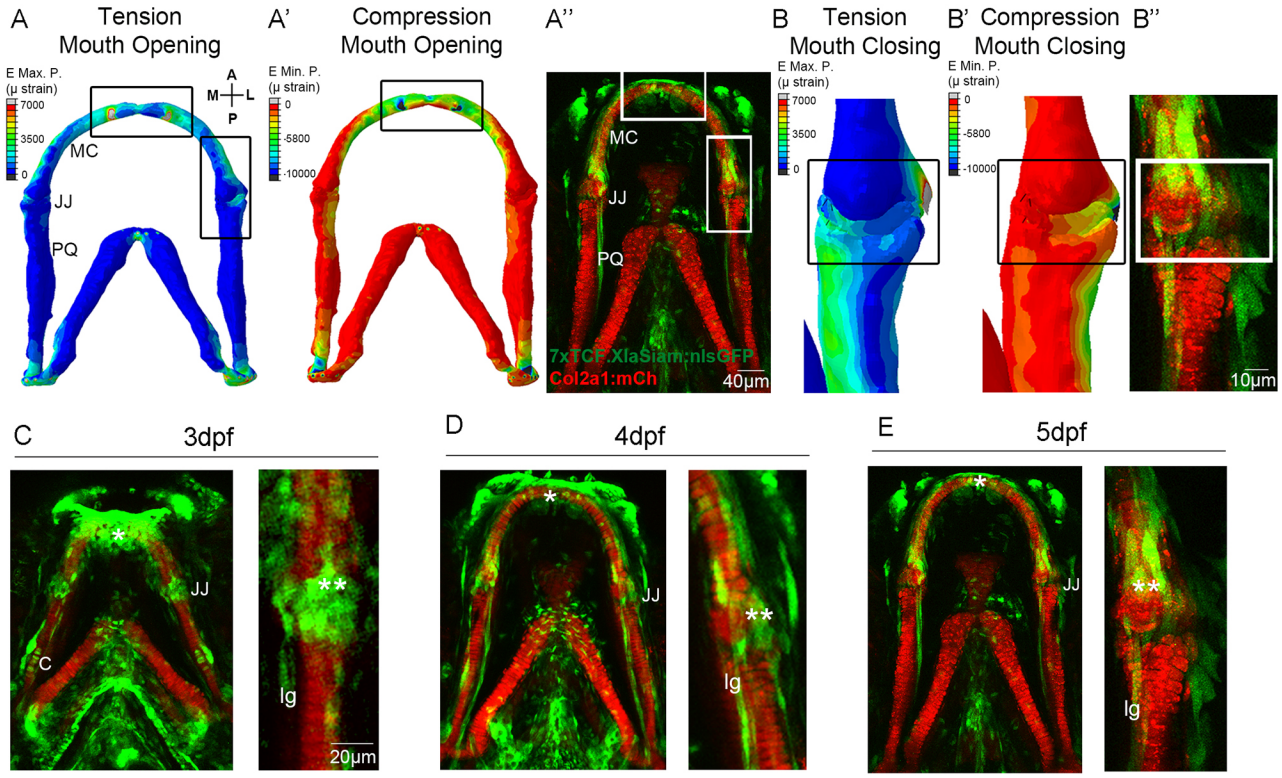

Fig. 1. Patterns of biomechanical strain and the location of Wnt-responsive cells at the zebrafish lower jaw between 3 and 5 dpf. (A,A′) Finite element (FE) model of maximum (E max. P., tension, A) and minimum (E min. P., compression, A′) principal strain on the zebrafish lower jaw during mouth opening at 5 dpf. (B,B′) FE model of maximum (E max. P., tension, B) and minimum (E min. P., compression, B′) principal strain on the jaw joint during mouth closure at 5 dpf. Colour key represents strain in microstrain (μstrain units). (A″,B″,C-E) *Tg(7xTCF.XlaSiam:nlsGFP)* and *Tg(Col2a1aBAC:mcherry)* transgenic zebrafish lines with, respectively, the Wnt-responsive cells (green) and cartilage (red) of the lower jaw labelled at 3 (C), 4 (D) and 5 dpf (A″,B″,E). (C-E) Left: lower jaw. Right and B″: jaw joint. (A,A′,B,B′) Reproduced from Brunt et al. (2015), where it was published under a CC-BY license (https://creativecommons.org/licenses/by/4.0/). A, anterior; P, posterior; M, medial; L, lateral; MC, Meckel's cartilage; JJ, jaw joint; PQ, palatoquadrate; C, cartilage; lg, ligament; *anterior MC; **jaw joint. Scale bars: 40 μm in A″; 10 μm in B″; 20 μm in C-E.

Development (2017) 144, 2798-2809 doi:10.1242/dev.153528

morphogenesis (Brunt et al., 2015). Using morphology, location and immunohistochemical labelling against ligaments and tendons, and chondrocyte markers we identified a heterogeneous population of GFP$^+$ cells (Fig. S1). This included chondrocytes at the jaw joint, visualised from a single *z*-slice through the joint (Fig. S1A), chondrocytes along the palatoquadrate (PQ) (Fig. 1C), and ligaments and tendons [which appear yellow when co-labelled for Tenascin C (Fig. 1C-E, Fig. S1B)]. Additional GFP$^+$ cells surrounding the jaw joint within a 10-15 µm *z*-slice range from the joint (Fig. 1C-E) were identified as joint-associated cells. These Wnt-responsive cells at the lower jaw are, therefore, not only located in areas subjected to high levels of tensile and compressive strain but include cell types known to respond to biomechanical stimuli, such as chondrocytes and ligaments.

Canonical Wnt signalling in the lower jaw is biomechanically controlled

To test whether canonical Wnt signalling in the jaw is mechanically controlled, zebrafish carrying transgenes for *Col2a1aBAC:mcherry* and *7xTCF.XlaSiam:nlsGFP* were immobilised from 3-5 dpf to prevent jaw movement, and *Tg(7xTCF.XlaSiam:nlsGFP)* GFP$^+$ signal was quantified by measuring the volume of segmented GFP$^+$ cells within a region of interest in the lower jaw (Fig. 2). A significantly reduced GFP$^+$ signal in the lower jaw at 5 dpf was present after a period of immobilisation, most notably at the jaw joint region (Fig. 2A,B), as shown by 3D render of the green channel in the area surrounding the jaw joint and PQ. At 5 dpf, the volume of GFP$^+$ signal surrounding the MC joint and PQ (Fig. 2C), and specifically in the jaw joint (Fig. 2D), was significantly reduced in immobilised zebrafish (Fig. 2C′,D′). The total number of GFP$^+$ Wnt-responsive cells in the jaw joint region was significantly reduced at 5 dpf (Fig. 2E,F) and there were significantly fewer GFP$^+$ ligament and/or tendon cells at 4 and 5 dpf (Fig. 2G). This demonstrates that loss of muscle activity affects canonical Wnt activity in the lower jaw, suggesting that Wnt signalling is biomechanically controlled.

Blocking canonical Wnt signalling leads to altered jaw joint morphology independently of muscle activity

We have previously shown that immobilising the jaw leads to abnormal joint formation (Brunt et al., 2015, 2016b). To test whether changes to Wnt activity affect jaw joint morphology, independently of movement, *Tg(Col2a1aBAC:mcherry)* zebrafish were exposed to the Wnt antagonist IWR-1 from 3 to 5 dpf. The addition of IWR-1 had no significant effect on the frequency of mouth movements compared with control (Fig. S2), i.e. jaw muscle activity was normal. However, IWR-1 treatment affects the functional morphology of the 5 dpf jaw joint, such that the medial region of the MC overlapped the PQ element, impeding smooth movement (Fig. 3A,A′). IWR-1 treatment caused the lateral interzone region to be significantly larger than control and the medial interzone region to be significantly reduced, owing to overlapping elements (Fig. 3B,B′). There was no effect on the total length of the jaw (Fig. S3A) or MC (Fig. S3B), suggesting that normal growth was not inhibited. However, the proportion of chondrocytes in the MC that were fully intercalated was significantly reduced (Fig. S3C), concurrent with a significant increase in the proportion of rounded chondrocytes in the 5 dpf jaw joint (Fig. S3D). This failure of intercalation and reduced cell maturation at the joint phenocopies what is previously seen in immobilised *nic* b107 mutants and anaesthetised zebrafish (Brunt et al., 2016b; Shwartz et al., 2012). Therefore, IWR-1 treatment, independently of muscle activity and joint movement, recapitulates cell behaviours seen after immobility.

Knockdown and mosaic knockout of Wnt16 leads to altered jaw joint morphology

Application of a Wnt antagonist (IWR-1) shows that a reduction in canonical Wnt activity leads to abnormal jaw joint morphogenesis. We took a candidate approach to identify Wnt pathway members that could transduce the mechanical signal into altered cell behaviour. Wnt16 has been previously reported to be expressed in mouse limb joints (Witte et al., 2009) and differentially regulated in mice lacking limb muscle (Rolfe et al., 2014), and Wnt16 overexpression in mouse joint synovium has been shown to activate canonical Wnt signalling in joint cartilage (van den Bosch et al., 2015). We used the previously described Wnt16 MO (Clements et al., 2011) to determine the effect of reduced Wnt16 on jaw and joint morphology. Wnt16 knockdown had no effect on the gross morphology of the zebrafish larvae (Fig. S4B) or on the frequency of jaw movement (data not shown). Wnt16 knockdown led to reduced levels of *lef1* mRNA in jaw cartilage elements such as the branchial arches (Fig. S5A,A′), while leaving other expression domains – such as the brain – intact (Fig. S5A,A′). Wnt16 morphants showed a significant reduction in *Tg(7xTCF.XlaSiam:nlsGFP)* GFP$^+$ signal volume in the jaw compared with control (Fig. S5B-E), demonstrating that Wnt16 activates canonical Wnt signalling in the lower jaw independently of jaw movement.

Wnt16 morphants show altered jaw joint morphology with an overlapping MC element (Fig. 3C,C′). At 3 dpf, Wnt16 morphants have a reduced interzone space on the medial side of the joint because of the overlap of the elements on the medial side (Fig. 3D,D′). Interzone interval measurements were, however, not significantly different from control at 5 dpf. This shows Wnt16 knockdown affects functional jaw joint morphology, but this is less severe than the effect seen in IWR-1-treated fish at 5 dpf. Wnt16 MO injection did not significantly affect the total jaw length or MC length at 5 dpf, showing that overall jaw growth was unaffected and Wnt16 knockdown very specifically affected only the joint region of the cartilage element (Fig. S3A,B), with no other discernible off-target effects. Mosaic Wnt16 knockout also leads to abnormal jaw joint morphology with an overlapping medial joint region, as visualised with Amira using a 3D render of the cartilage reporter (Fig. 3E1′,E2′), but also does not affect normal jaw growth and development. Unlike IWR-1 treatment, Wnt16 knockdown and mosaic knockout does not significantly affect cell intercalation (Fig. 3E, Fig. S3C,D). Wnt16 is therefore important for joint morphology, but does not affect cell intercalation.

Cell proliferation, migration and changes to cell morphology contribute to jaw joint morphogenesis

In order to understand the cell behaviour changes that shape the joint, we tracked cells at the joint in individual larvae. As continuous time-lapse imaging to follow the process of joint morphogenesis would require long-term immobilisation, which would in turn lead to abnormal morphogenesis, we used zebrafish carrying both *Tg(Sox10:GAL4-VP16)* and *Tg(UAS:Kaede)* transgenes to track populations of Kaede-expressing joint cells from 3 to 5 dpf. A small batch of 10-12 cells at the medial side of the joint were photoconverted at 3 dpf to irreversibly switch the labelling from green to red, making it possible to follow the cells over time. Medially located cells close to the retroarticular process (RAP) were chosen as the medial region of the joint is most affected by immobilisation and Wnt abrogation (Fig. 3) (Brunt et al., 2015). Red

Development (2017) 144, 2798-2809 doi:10.1242/dev.153528

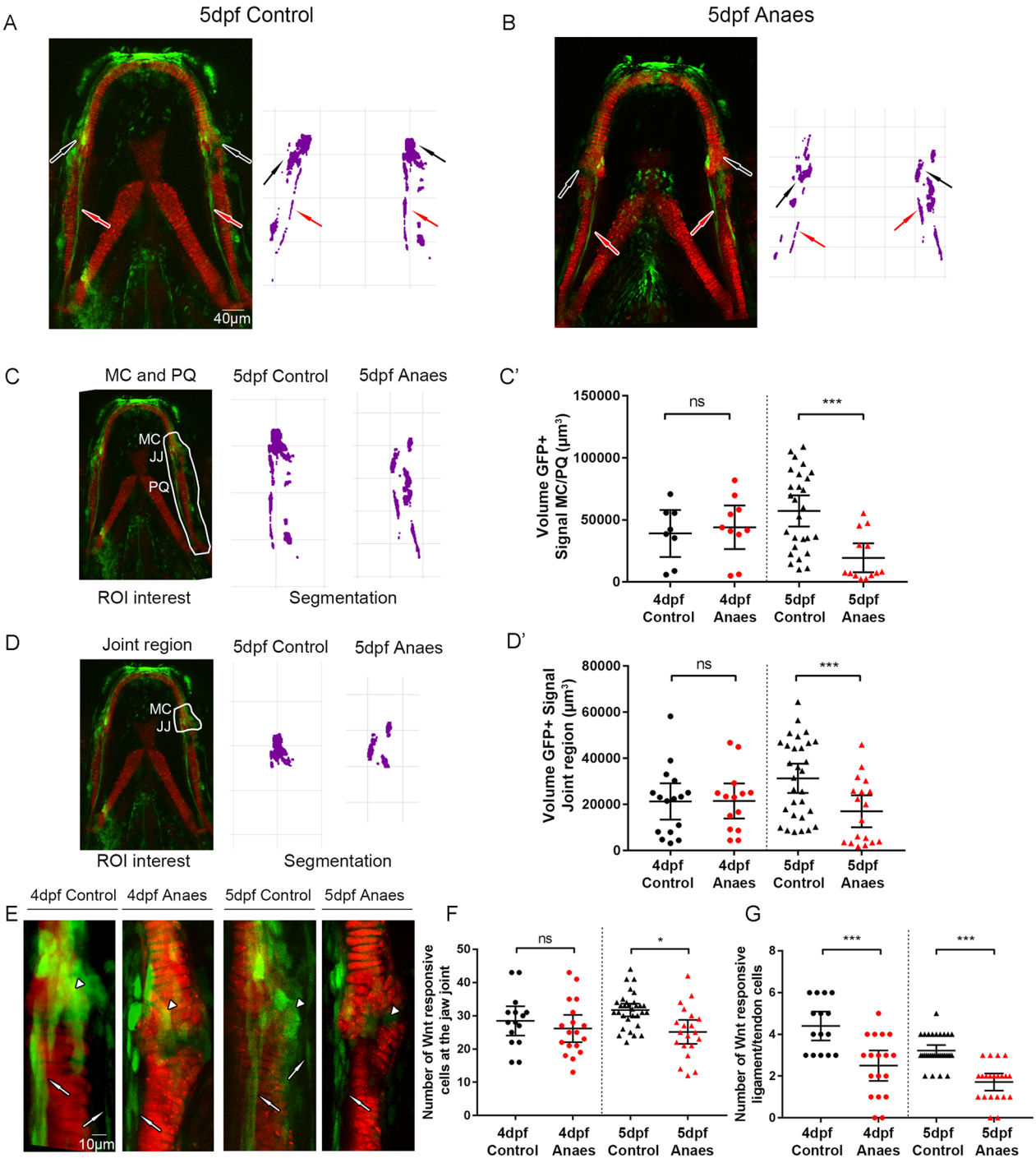

Fig. 2. Immobilisation causes a reduction in canonical Wnt signalling activity at the zebrafish lower jaw. (A,B) *Tg(7xTCF.XlaSiam:nlsGFP)* and *Tg(Col2a1aBAC:mcherry)* transgenic zebrafish lines were used to visualise Wnt-responsive cells (green) and chondrocytes (red) in 5 dpf control (A) and 5 dpf immobilised (B) zebrafish. Anaes, anaesthetised larvae from 3 to 5 dpf. Left: merge of *Tg(7xTCF.XlaSiam:nlsGFP)* and *Tg(Col2a1aBAC:mcherry)*. Right: segmentation of GFP signal. Black arrows indicate cells surrounding the jaw joint; red arrows indicate ligaments and tendons. (C) Left: volume analysis of *Tg(7xTCF.XlaSiam:nlsGFP)* GFP$^+$ signal at the region of interest (ROI) from six intercalating cells above the Meckel's cartilage (MC) jaw joint (JJ) and along the full extent of the palatoquadrate (PQ) (white line). Right: segmentation of GFP$^+$ signal volume from the ROI in 5 dpf control and anaesthetised zebrafish. (C′) Volume (μm^3) of GFP$^+$ signal at the MC joint and along the PQ in 4 and 5 dpf control and anaesthetised zebrafish (*n*=8, 10, 27 and 13 joints). (D) Left: volume analysis of *Tg(7xTCF.XlaSiam:nlsGFP)* GFP$^+$ signal at the ROI from six intercalating cells above the MC jaw joint to the interzone (white line). Right: segmentation of GFP$^+$ signal volume from the ROI in 5 dpf control and anaesthetised zebrafish. (D′) Volume (μm^3) of GFP$^+$ signal at the MC joint in 4 and 5 dpf control and anaesthetised zebrafish (*n*=16, 14, 30 and 18 joints). (E) *Tg(7xTCF.XlaSiam:nlsGFP)* and *Tg(Col2a1aBAC:mcherry)* transgenic zebrafish with Wnt-responsive cells and cartilage of the lower jaw at the jaw joint labelled in 4 and 5 dpf control and anaesthetised zebrafish. White arrowheads indicate joint-associated GFP$^+$ cells. White arrows indicate ligament and tendon GFP$^+$ cells. (F) Number of GFP$^+$ cells in 4 and 5 dpf control and anaesthetised zebrafish in a 50×80 μm area surrounding the jaw joint (*n*=15, 18, 31 and 13 joints). (G) Number of ligament and tendon GFP$^+$ cells in 4 and 5 dpf control and anaesthetised zebrafish at the jaw joint. (*n*=15, 18, 31 and 13 joints). Kruskal–Wallis tests were carried out for statistical analysis in C′,D′,G and one-way ANOVA in F. ns, not significant, *$P\leq0.05$, ***$P\leq0.001$. Data are mean and 95% confidence interval.

Development (2017) 144, 2798-2809 doi:10.1242/dev.153528

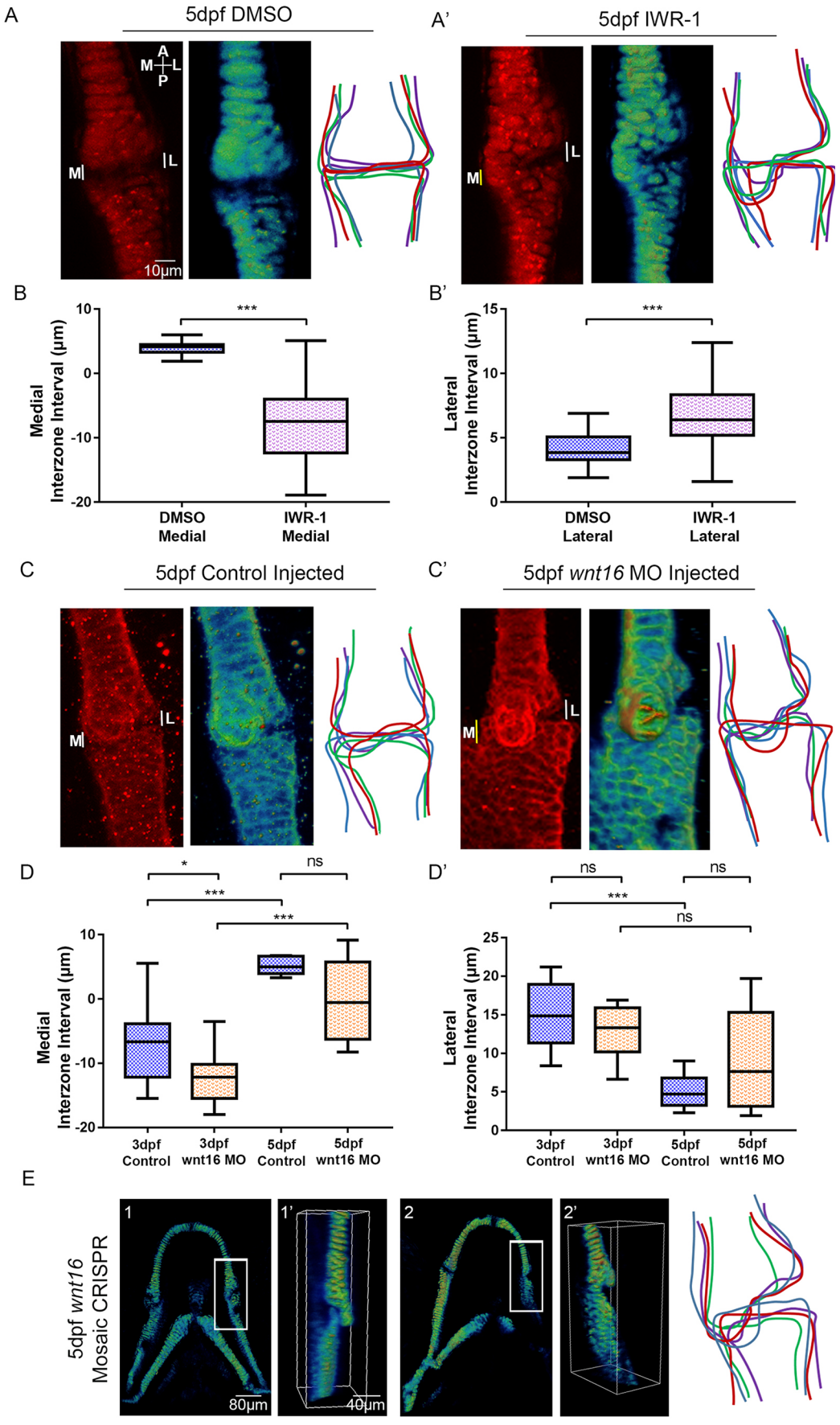

Fig. 3. See next page for legend.

Development (2017) 144, 2798-2809 doi:10.1242/dev.153528

Fig. 3. Manipulation of Wnt affects zebrafish jaw joint morphology. (A,A′) 5 dpf DMSO control (A) and 5 dpf 20 µM IWR-1-treated (from 3-5 dpf) (A′) zebrafish jaw joint morphology. Left: *Tg(Col2a1aBAC:mcherry)* transgenic zebrafish line marks the cartilage of the jaw joint. Middle: 3D volume rendering of jaw joint. Right: outlines of four representative jaw joints. A, anterior; P, posterior; M, medial; L, lateral. White lines indicate interzone interval measurements between MC and PQ; yellow line indicates overlapping interval between MC and PQ. (B,B′) Interzone intervals (µm) between the MC and PQ on the medial (B) and lateral (B′) regions of the jaw joint in 5 dpf DMSO and IWR-1-treated zebrafish. Negative values represent an overlap of MC/PQ elements (n=42 and 45 joints). Two-tailed Student's t-tests were performed for B,B′. (C,C′) 5 dpf control-injected (C) and Wnt16 morpholino (MO)-injected (C′) zebrafish jaw joint morphology. Left: immunohistochemical stain of the jaw joint region. Middle: 3D volume rendering of the jaw joint. Right: outlines of four representative jaw joints. (D,D′) Interzone intervals (µm) between the MC and PQ on the medial (D) and lateral (D′) regions of the jaw joint in 5 dpf control-injected and Wnt16 MO-injected zebrafish. Negative values represent an overlap of MC/PQ elements (n=8, 11, 6 and 8 joints). One-way ANOVA calculations were performed (D,D′). ns, not significant, *P≤0.05, ***P≤0.001. Data are mean and 95% confidence interval. (E) 3D volume rendering of 5 dpf injected CRISPR/Cas9 mosaic *wnt16* knockout *Tg(Col2a1aBAC:mcherry)* larvae (1,2) (n=12 animals). Image was enlarged and rotated to best show the jaw joint (1′,2′). Right: outlines of four representative jaw joints.

photoconverted cells in the medial joint at 3 dpf spread along the anterior-posterior axis of the jaw joint by 5 dpf, contributing to the change in joint shape (Fig. 4A,C). Some cells within this group remain part of the MC; however, other cells migrate to the PQ. Between 3 and 5 dpf there is a 97.5% mean increase in the area occupied by red cells (Fig. 4E). Cell counts reveal that this area increase is, in part, due to an increase in cell number from 3 to 5 dpf (Fig. 4F), showing that proliferation contributes to changes in joint shape. BrdU pulse-chase experiments show that proliferation events mainly occur between 4 and 5 dpf (Fig. S6A-A″,D). From 3 to 5 dpf, cell morphology changes are also observed, with elongated perichondrial cells migrating from the original pool of round photoconverted cells to form the perichondrium (Fig. 4A,A′,C,C′). These data demonstrate that cells at the joint are highly dynamic, with migration, proliferation and changes to cell type and morphology all contributing to normal joint morphogenesis.

We then tracked joint cells in immobilised larvae to investigate whether cell behaviour is altered in these larvae. In immobilised larvae, red photoconverted cells remained largely static between 3 and 5 dpf (Fig. 4B,B′) and the percentage increase in the area occupied by red cells was significantly reduced compared with control (Fig. 4E). The percentage increase in the number of cells inheriting red Kaede at the joint between 3 and 5 dpf was also significantly reduced (Fig. 4F). Therefore, mechanical stimuli are required to trigger normal cell behaviours such as proliferation and migration in order to shape the joint correctly.

Wnt16 controls cell proliferation and migration in the jaw joint

To investigate whether Wnt16 plays a role in controlling cell behaviours in the joint, a group of 10-12 red photoconverted cells per fish were tracked in Wnt16 morphants and Wnt16 mosaic CRISPR knockouts. From 3 to 5 dpf, the spread of red photoconverted cells observed in control injected larvae did not take place in Wnt16 morphants or in Wnt16 mosaic CRISPR knockouts (CRISPants) (Fig. 4C-D′, Fig. S7A-B′). The percentage increase in red cell area was significantly reduced in morphants and CRISPants compared with control larvae (Fig. 4D,E, Fig. S7C). The percentage increase in cell number was significantly reduced in morphants compared with control (Fig. 4F) and the number of BrdU-positive cells in the joint was also significantly less (Fig. S6C, D). This shows that Wnt16 controls cell behaviours, including proliferation and migration, during joint morphogenesis. Interestingly, the effect of Wnt16 knockdown on chondrocyte migration and proliferation is highly joint specific, as there was no significant change in cell behaviour in the more mature intercalated region (Figs S6B′,C′,E and S8), further confirming specificity of the MO and CRISPR.

Next, we used zebrafish with the *ubi:Zebrabow* transgene under the control of *Sox10:cre* to track individual cells, in order to unpick individual cell behaviours taking place during joint morphogenesis. At 3 dpf, the retroarticular process (RAP) contains cells with different colour profiles, which could be tracked (Fig. 5A-A″). In control zebrafish, cells that had undergone proliferation between 3 and 5 dpf were observed in the joint (Fig. 5B). Cell morphology changes were also observed (Fig. 5B′).

However, in IWR-1-treated and Wnt16 morphant larvae, cell proliferation was not observed in the RAP between 3 and 5 dpf (Fig. 5C-D′). In IWR-1-treated zebrafish, the cells of the RAP are less plastic, with minimal changes to cell morphology between 3 and 5 dpf (Fig. 5C′). In Wnt16 morphants, cell morphology changes were not affected, as the cells of the RAP became enlarged or changed shape (Fig. 5D′). Both cellular processes are affected by IWR-1 application, and proliferation is affected by Wnt16MO knockdown. This shows that Wnt16 controls cell proliferation and migration in the joint, but suggests cell morphology changes may be controlled by other members of the Wnt pathway.

DISCUSSION

Mechanical input has previously been shown to affect joint morphogenesis in a number of species ranging from mouse to fish (Brunt et al., 2015, 2016b; Kahn et al., 2009; Nowlan et al., 2010b; Rolfe et al., 2013). However, the identities of the downstream signalling pathways drive the cell behaviours that shape the joint in response to these forces, which are less well characterised. By tracking cell behaviour dynamically in the joint for the first time in larvae subjected to mechanical, genetic and pharmacological perturbations, we show that joint morphology is shaped through a combination of cell morphology changes, migration and proliferation. Cells in the medial region of a joint, which are most affected in mechanical loss models, normally spread and migrate anterior and posterior to their original location to remain part of Meckel's cartilage or to become part of the palatoquadrate. In chick and in mouse, it has been shown that progenitor cells from outside the joint can move into the developing joint to form articular cartilage (Pacifici et al., 2006; Shwartz et al., 2016). Cell proliferation in the jaw joint mainly occurs from 4 to 5 dpf, and cell morphology changes also contribute to the overall shape of the joint. We also show that interzone cells can give rise to mature chondrocytes or form the perichondrium. This is the first study to describe the dynamic cell behaviours occurring in joints in individually tracked animals and therefore gives a dynamic insight into morphogenesis of the joint *in vivo*. We show that removal of muscle force leads to reduced proliferation in the zebrafish joint, analogous to the situation in chicks and mice (Jahan et al., 2014; Kahn et al., 2009; Roddy et al., 2011). Our work also builds on previous work showing the relevance of the zebrafish as a model for synovial joint development (Askary et al., 2016).

Here, we demonstrate that canonical Wnt signalling, and Wnt16, act downstream of muscle activity to transduce the mechanical signals into the cell behavioural changes, such as proliferation and migration, that shape the joint. It has been previously shown in

Development (2017) 144, 2798-2809 doi:10.1242/dev.153528

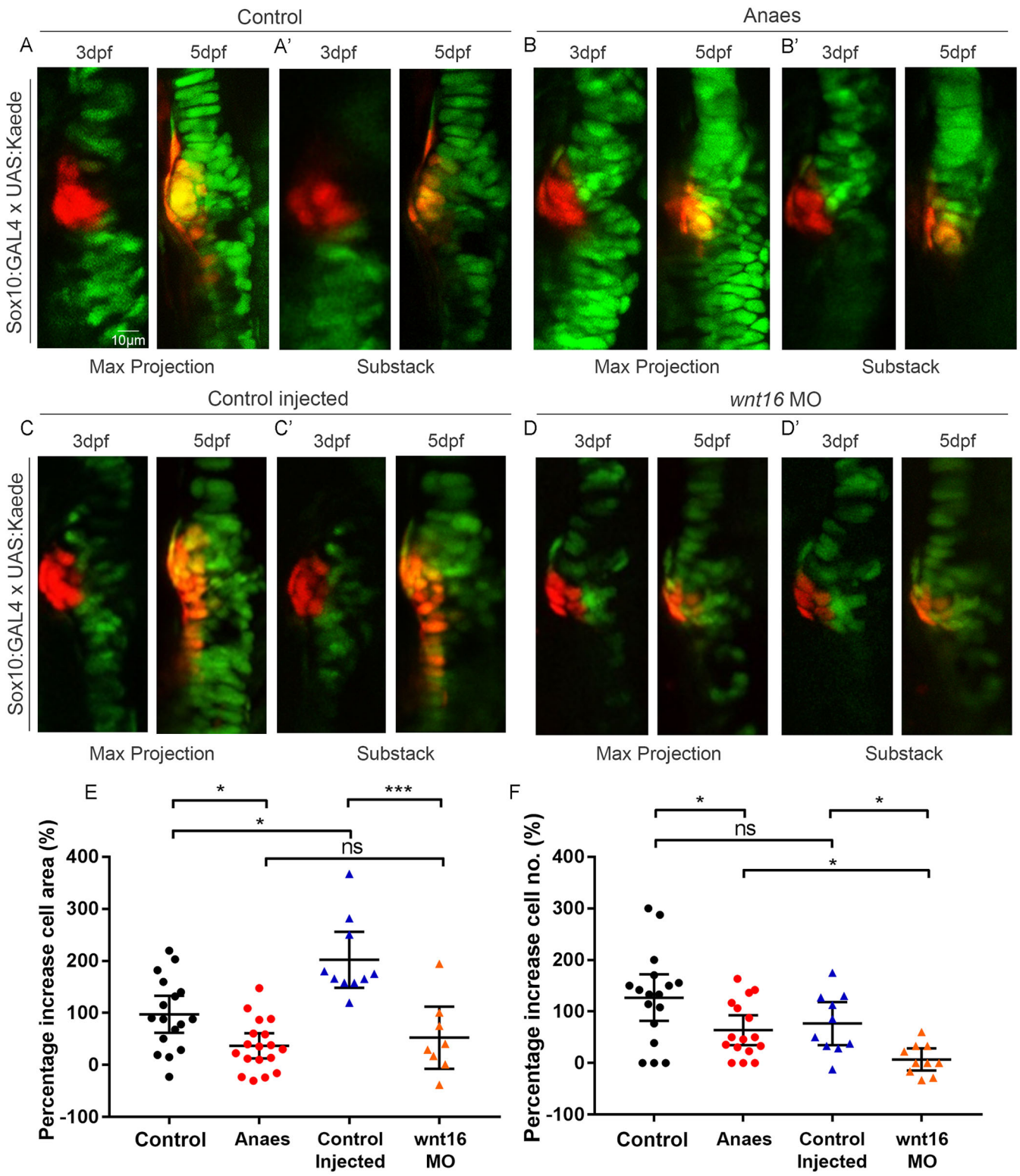

Fig. 4. Immobilisation and Wnt16 knockdown affects cell proliferation and migration at the medial region of the jaw joint between 3 and 5 dpf. (A-D′) *Tg(Sox10:GAL4-VP16)* and *Tg(UAS:Kaede)* transgenic line drives expression of Kaede protein (green) in the cartilage of control (A), anaesthetised (B), control-injected (C) and Wnt16 morpholino (MO)-injected (D) zebrafish. Maximum projections of the jaw joint from stacks of tiff images (A,B,C,D) and single slice/substacks through the same jaw joint to show cell morphology (A′,B′,C′,D′) are represented. At the jaw joint, medially located Kaede-expressing cells are photoconverted to red Kaede at 3 dpf (left panels). Right panels show jaw joints from the same larva re-imaged at 5 dpf. Photoconverted cells appear red/orange owing to presence of photoconverted red Kaede and expression of newly made green Kaede protein under control of the *sox10* promoter. (E) Percentage increase in total area of cells expressing photoconverted red Kaede between 3 and 5 dpf in control, anaesthetised, control-injected and Wnt16 MO-injected zebrafish jaw joints (n=17, 18, 10 and 8 joints, respectively). (F) Percentage increase in number of cells expressing photoconverted red Kaede between 3 and 5 dpf in control, anaesthetised, control-injected and Wnt16 MO-injected zebrafish jaw joints (n=17, 16, 10 and 10 joints, respectively). Kruskal–Wallis tests were performed for E,F. ns, not significant, *P≤0.05, ***P≤0.001. Data are mean and 95%CI.

Development (2017) 144, 2798-2809 doi:10.1242/dev.153528

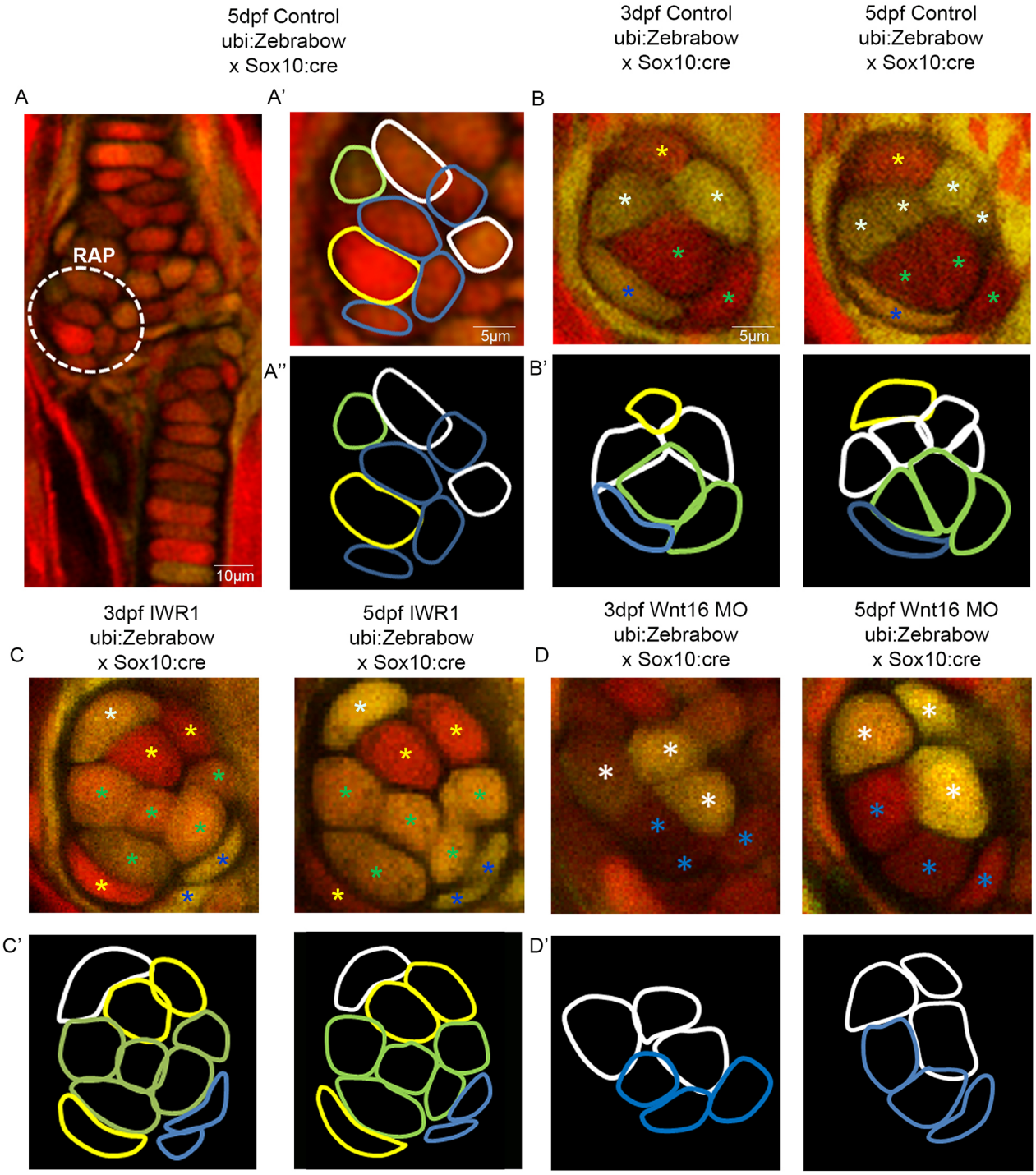

Fig. 5. Wnt manipulation affects cell proliferation and cell morphology at the jaw joint, revealed using the Zebrabow transgenic line. (A-A″): *Tg(ubi:Zebrabow)* and *Tg(Sox10:cre)* transgenic lines generate multiple colours of fluorescence in zebrafish cartilage, including at the region of interest at the retroarticular process (RAP) (white dotted line). Cell outlines were created at the RAP: (A′) RAP cell outlines overlaid with confocal image; (A″) cell outlines. (B,C,D) 3 and 5 dpf *Tg(ubi:Zebrabow)* and *Tg(Sox10:cre)* control (B), IWR-1-treated (C) and Wnt16 MO-injected zebrafish (D) (n=10, 11 and 20 joints). The RAP of the MC jaw joint is shown. Asterisks of different colours mark cells at 3 and 5 dpf (indicating re-identification and cell division events). (B′,C′,D′) Outlines of individual cells in the RAP of the MC jaw joint, identified in control (B′), IWR-1-treated (C′) and Wnt16 MO-injected (D′) *Tg(ubi:Zebrabow)* and *Tg(Sox10:cre)* transgenic zebrafish. Outline colour of individual cells in B′,C′,D′ matches the asterisk colours in B,C,D.

mesenchymal stem cell *in vitro* preparations that mechanical strain can activate Wnt signalling (Arnsdorf et al., 2009; Haudenschild et al., 2009; Rolfe et al., 2014) and transcriptomic studies in muscle-less mice have demonstrated changes in expression of Wnt pathway members (Rolfe et al., 2014). We show that canonical Wnt signalling is activated in cells associated with the zebrafish jaw joint, which are located in regions that are under high levels of strain. We demonstrate that canonical Wnt signalling in the jaw joint, and in ligaments, is mechanosensitive, with significant reductions in the number of Wnt GFP^{+} cells in the joint and in associated connective

Development (2017) 144, 2798-2809 doi:10.1242/dev.153528

tissues when force is lost. Previous work in zebrafish has shown that craniofacial muscle is not required for induction of expression of early markers of tendon and ligament, but that muscle attachment is required for maintenance of expression at 72 hpf (Chen and Galloway, 2014). Immobilisation in our study starts somewhat later (from 72 hpf) but we can still identify changes in the ligaments and a reduction in Wnt signalling activity at 4 and 5 dpf. This strongly suggests that Wnt signalling plays a mechanosensitive role in later tendon and ligament maturation. Wnt and/or β-catenin has been linked to a mechanosensitive role in controlling expression of osteogenic genes in cells derived from human periodontal ligaments (Chen et al., 2017; Zhang et al., 2016), and our work suggests that Wnt is likely to play a role in maturation of other craniofacial ligaments. We observe that canonical Wnt signalling manipulation causes abnormalities in joint morphology. This occurs even under conditions where muscle activity is still present, demonstrating that Wnt signalling acts downstream of muscle activity to cause changes in joint shape. How precisely Wnt senses strain remains an unresolved issue; however possibilities include via mechanosensitive primary cilia [we observe primary cilia labelled by arl13b in the developing zebrafish joint (C.L.H. and D. J. Bergen, unpublished)], via activation of ion channels (Li et al., 2002) or integrins (reviewed by Ingber, 2006), or potentially via Frizzled receptors themselves, where shear-activated Frizzled receptors interact with LRP5/6 to activate downstream signals (Rotherham and El Haj, 2015).

We show that Wnt16 is important for accurate shaping of the joint by controlling cell proliferation and migration events at the joint. Unlike reduction in broad canonical Wnt signalling, abrogation of Wnt16 had no effect on cell behaviours such as proliferation, migration and intercalation of maturing chondrocytes anterior to the jaw joint, acting in a highly joint-specific fashion. Therefore, other Wnt ligands are likely to be responsible for chondrocyte intercalation in Meckel's cartilage, as is the case for chondrocyte intercalation in chick growth plates (Li and Dudley, 2009; Rochard et al., 2016) and during zebrafish palate morphogenesis (Dougherty et al., 2013; Kamel et al., 2013; Rochard et al., 2016). Wnt16 has been previously implicated in joint formation, bone homeostasis and remodelling (Gori et al., 2015; Guo et al., 2004; Kobayashi et al., 2016) and is expressed at the developing joint in mouse models (Guo et al., 2004; Witte et al., 2009). It has been shown to be required for proliferation, differentiation and specification in other cell types, such as haematopoietic stem cells, osteoclasts, osteoblasts and keratinocytes (Clements et al., 2011; Kobayashi et al., 2015; Ozeki et al., 2016; Teh et al., 2007). Wnt16 is upregulated following mechanical injury in *ex vivo* human cartilage (Dell'Accio et al., 2008), and following mechanical loading of the tibia in mice (Wergedal et al., 2015). Expression levels of Wnt16 are upregulated in 'muscle-less' *splotch* mice compared with control (Dell'Accio et al., 2008; Rolfe et al., 2014; Wergedal et al., 2015). We show that Wnt16 controls proliferation and migration of a small number of cells in the joint, which are crucial for normal joint morphology to be generated.

The role of Wnts, in particular Wnt16, in controlling joint morphogenesis during development may have a longer-term impact on joint health. The formation of abnormal joint morphology during development is a crucial risk factor for the onset of osteoarthritis (Baker-LePain and Lane, 2010). Wnt-related genes, such as the Wnt antagonist *FRZB* are implicated in accurate joint shaping (Baker-Lepain et al., 2012). Wnt16 has been linked to the relationship between hip geometry and the risk of osteoarthritis onset (Garcia-Ibarbia et al., 2013). Wnt16 is upregulated in joints with moderate to severe osteoarthritis along with increased nuclear β-catenin expression (Dell'Accio et al., 2008). Upregulation is also documented after mechanical injury (Dell'Accio et al., 2008). Our study builds on these findings to suggest that the relationship found between osteoarthritis risk, joint shape and Wnt16 may stem from its role in activating early joint cell behaviours that affect the functional joint shape.

MATERIALS AND METHODS

Zebrafish husbandry and transgenic lines

Zebrafish were maintained as previously described (Westerfield, 2000). Experiments were approved by the local ethics committee (the Animal Welfare and Ethical Review Body of the University of Bristol) and granted a UK Home Office project licence. Transgenic lines *Tg(7xTCF.XlaSiam:nlsGFP)* (Moro et al., 2012), *Tg(Col2a1aBAC:mcherry)* (Hammond and Schulte-Merker, 2009), *Tg(Sox10:GAL4-VP16)* (Lee et al., 2013), *Tg(UAS:Kaede)* (Hatta et al., 2006), *Tg(ubi:Zebrabow)* (Pan et al., 2013) and *Tg(-4.7Sox10:cre)* (Rodrigues et al., 2012) have been previously described. Larvae from the same lay were randomly assigned to different treatment groups.

Pharmacological treatment

Fish were anaesthetised between 3 and 5 dpf with 0.1 mg/ml MS222 (Tricaine methanesulfonate) (Sigma) diluted in Danieau solution. MS222 and Danieau solution were refreshed twice daily. 20 µM IWR-1 (Sigma) was diluted in Danieau solution and replaced daily from 3 dpf to 5 dpf.

Finite element models

Meshes for 5 dpf finite element (FE) models have been previously published (Brunt et al., 2015, 2016a). Loads for jaw opening (protractor hyoideus and intermandibularis anterior muscles) and jaw closure (adductor mandibulae muscles) were applied to predict tensile and compressive strains. FE results are displayed as colour contour plots of maximum and minimum strain.

Wnt-responsive cell counts and area

Image stacks from jaws labelled with *Tg(7xTCR.ZXlaSiam:nlsGFP)* and *Tg(Col2a1aBAC:mcherry)* were imported into Fiji (Schindelin et al., 2012). Wnt-responsive cells with ligament and tendon morphology along the palatoquadrate (PQ) element were counted. All Wnt-responsive cells surrounding the jaw joint within a 50×80 µm area were counted.

A custom script was written in MATLAB (version 2015a; Mathworks) so that a selected area of *Tg(7xTCF.XlaSiam:nlsGFP)* GFP^+ signal could be determined. Areas of interest included: (1) the area of Meckel's cartilage (MC) (from six intercalating cells above the MC joint) plus the PQ; and (2) the joint region (from six intercalating cells above the MC joint to the MC interzone). Coarse regions of interest were initially manually identified from maximum intensity projections of the image stack and subsequently segmented in 3 dimensions (3D) based on the MATLAB implementation of Otsu's threshold (Otsu, 1979). All voxels within a user-selected region of interest with intensity values above the threshold were classified as a single object. An alpha shape was calculated for each segmented object (Edelsbrunner et al., 1983) using MATLAB's automatically determined surface radius. Volumes for each object were measured using the method provided by the MATLAB alpha shape class.

Whole-mount immunohistochemistry

Whole-mount immunohistochemistry was carried out as previously described (Hammond and Schulte-Merker, 2009). Larvae to be stained for BrdU were treated with 2N HCl for 1 h at 37°C. The following primary antibodies previously used in zebrafish (Table S1) were used: chicken anti-GFP (ab13970, Abcam, 1:500 dilution); rabbit anti-tenascin C (USBI142433, US Biological, 1:300 dilution); mouse anti-BrdU (B8434, Sigma, 1:100 dilution); rabbit anti-collagen II (ab34712, Abcam, 1:200 dilution); and mouse anti-collagen II (II-II6B3) (AB528165, Developmental Studies Hybridoma Bank, 1:200 dilution). Secondary

Development (2017) 144, 2798-2809 doi:10.1242/dev.153528

antibodies used were Dylight 550 goat anti-mouse IgG (84540); Dylight 488 goat anti-mouse IgG (35502); Dylight 550 goat anti-rabbit IgG (84541); Dylight 488 goat anti-chicken IgY (SA5-10070) (all from ThermoFisher Scientific, 1:500 dilution).

Joint outline and interzone interval analysis

Tiff images of *Tg(Col2a1aBAC:mcherry)* transgenic labelled joints were imported into Powerpoint. The draw tool was used to draw around four representative joints for each condition and overlaid for analysis. Amira (version 6.3) was used to 3D render image stacks from *Tg(Col2a1aBAC:mcherry)* and anti-collagen II-stained jaw cartilage; colour coding of images reflects pixel intensity.

The interval between MC and PQ cartilage elements on the medial and lateral side of the jaw joint were measured from tiff images in LAS AF Lite software. Negative values correspond to instances of overlapping cartilage elements.

Kaede protein photoconversion

Double transgenic *Tg(Sox10:GAL4-VP16)×Tg(UAS:Kaede)* zebrafish larvae at 3 dpf were mounted ventrally onto coverslips in 0.3% agarose under MS222 anaesthetic. The FRAP wizard setting on Leica LAS software was used to photoconvert Kaede-expressing cells of interest from green to red fluorescence on a Leica SP5 or SP8. Briefly, a region of interest (ROI) was drawn using the selection tools, on the medial regions of Meckel's cartilage joint or the intercalating cell region of MC. A wavelength of 405 nm was used to photoconvert cells in the ROI at 8% laser power for 10 s. Following photoconversion, larvae were removed from agarose and flushed with Danieau solution until resumption of movement. Each larva was kept separately for individual identification. Larvae were left to develop normally or anaesthetised with MS222 and reimaged at 5 dpf. Daughter cells inherit irreversibly photoconverted red Kaede protein after cell division (Mutoh et al., 2006).

Photoconverted cell number and area change

Image stacks containing the red channel were imported into Fiji software (Schindelin et al., 2012) and red cell numbers were counted at 3 and 5 dpf, and percentage increase in cell number calculated.

The image stacks were saved as a tiff file. A Fiji plug-in designed to segment a thresholded level of red cells was used to calculate the combined area of red cells; these areas were compared from the individual larvae from 3 to 5 dpf. The percentage increase in cell area was calculated.

Jaw and element length, and the ratios of cell type in the MC element

Confocal images of jaw joints labelled with *Tg(Col2a1aBAC:mcherry)* were loaded into Fiji (Schindelin et al., 2012). The length (µm) of the jaw was measured from anterior MC to posterior palatoquadrate using the line tool. The length of the MC element was measured using the freehand line tool from the anterior region of MC to the MC jaw joint. The proportion of the length (µm) of the MC comprising rounded cells or intercalating cells was measured in Fiji using the freehand line tool. The ratio of the length of the MC occupied by varying cell types compared with the full MC length was then calculated.

BrdU

Larvae were treated with 3 mM BrdU (Sigma) diluted in Danieau solution from 3 to 4 dpf or from 4 to 5 dpf. After treatment, larvae were washed four times for 5 min each in Danieau solution then fixed with 4% PFA overnight at 4°C. Larvae were then immunohistochemically stained for BrdU using the antibody already described.

Zebrabow

Double transgenic (*Tg(Ubi:Zebrabow)*) and *Tg(Sox10:Cre)* zebrafish larvae express a variety of different fluorescent protein combinations in the cells of the developing cartilage. This allows individual cells to be tracked as they migrate or divide. *Tg(Sox10:Cre)×Tg(Ubi:Zebrabow)* double transgenic zebrafish at 3 dpf were mounted in 0.3% agarose on coverslips in dishes and covered with Danieau solution containing MS222. The larvae were imaged on a Leica Multiphoton microscope using a 25× water-dipping lens. Three fluorescence channels were collected individually (YFP, RFP and GFP). Larvae were returned to Danieau solution in individual dishes and either left to develop normally or anaesthetised with MS222 until 5 dpf, then reimaged.

Wnt16 morpholino knockdown

A Wnt16 splice-blocking morpholino (MO) (Gene Tools), AGGTTAGTTCTGTCACCCACCTGTC, was used to knockdown Wnt16 protein as previously described (Clements et al., 2011). Wnt16 or control morpholino (5 ng) was injected with rhodamine dextran and 0.2 M potassium chloride into one-cell stage *Tg(Sox10:GAL4-VP16)×Tg(UAS:Kaede)* embryos using a picospritzer III (Parker) microinjector.

RNA extraction and making Wnt16 cDNA

Failure of splicing after Wnt16 MO injection was confirmed by PCR (Fig. S4A). Total RNA was extracted from pooled and homogenised 3 dpf Wnt16 MO-injected and control non-injected larvae using a Nucleospin RNA II kit (Macherey-Nagel). cDNA was produced from 1 µg RNA via reverse transcription using M-MLV reverse transcriptase (Promega). cDNA was amplified by PCR using Wnt16 primers [forward, ACTAAAGAGAC-AGCTTCATCC; reverse, AACTCATCTTTGGTGATAGGC (Eurofins Genomics)] (Clements et al., 2011) and Taq polymerase (Roche). PCR conditions have been previously described (Clements et al., 2011).

Wnt16 CRISPR mosaic knockout

CRISPR target sequences were selected using CRISPscan track from UCSC Browser (danRer10) (Moreno-Mateos et al., 2015) and were based on high scores and proximity to the first exon of Wnt16 (Fig. S9A). Two sequences targeting exon 2 were selected: guide1, GGAGGAGTGCCCGAGAAGTT (score 73-chr4:10708367-10708389); and guide2, GGTGGAACTGCTC-GACCCGA (score 64-chr4:10708367-10708389). gRNA antisense oligonucleotide sequences (5′-3′) were designed as follows: AAAGCA-CCGACTCGGTGCCACTTTTTCAAGTTGATAACGGACTAGCCTTAT-TTTAACTTGCTATTTCTAGCTCTAAAAC - N20 - **CTATAGTGAGT-CGTATTA**CGC, with the T7 promoter shown in bold and N20 indicating the reverse complement of targeting sequence, as described previously (Hruscha et al., 2013). *In vitro* transcription was carried out annealing gRNA antisense oligonucleotide to T7 primer (TAATACGACTCACTA-TAG; 5 min at 95°C, cooled at room temperature) followed by transcription using the Ambion MEGAshortscript-T7 kit. Injection mix was prepared to a final concentration of 200 ng/µl of gRNA and 600 ng/µl of GeneArt Platinum Cas9 nuclease (Invitrogen) and incubated for 10 min at room temperature. The solution (1pl) was injected into the cell of eggs at the one-cell stage (Fig. S9B). To check gRNA efficiency, DNA was extracted from individual larvae at 48 hpf followed by PCR amplification (Wnt16 F, GCCTGGTTATGGCATTTCAA; Wnt16 R, AAAACAAAACGTAAAT GTGAGACA) and fragment length analysis (ABI 3500) (Fig. S9B), as described previously (Carrington et al., 2015). After selecting the most efficient gRNA [>90% of injected embryos subjected to fragment analysis showed indel mutations in Wnt16 (e.g. Fig. S9B) n=45], injections were carried out in eggs from incrosses of *Tg(Sox10:GAL4-VP16);Tg(UAS:Kaede)* or *Tg(Col2a1aBAC:mcherry)* followed by Kaede photoconversion and imaging.

Mouth movements

Zebrafish anaesthetised with MS222 were mounted laterally on coverslips in 1% agarose. Forceps were used to remove agarose from around the head and Danieau solution was repeatedly flushed over the agarose-free cavity around the head until normal jaw movements resumed. The number of jaw movements in 1 min were recorded, using a stereo microscope.

In situ hybridisation

In situ hybridisation was performed as described previously (Thisse and Thisse, 2008), using 100 ng of *lef1* probe diluted into hybridisation buffer on 3 dpf larvae. *lef1* plasmid in a pBS-SK vector with ampicillin resistance was

Development (2017) 144, 2798-2809 doi:10.1242/dev.153528

delinearised using *Eco*RI and transcribed using T7. Samples were stored in 70% glycerol and whole-mount larvae imaged using a stereo microscope or jaws were dissected and imaged using a compound microscope.

Statistics

Statistics were performed using SPSS software. Student *t*-test and Mann–Whitney U-test were used for comparisons between parametric and non-parametric data, respectively. One-way ANOVA and Kruskal–Wallis tests were used to make multi-comparisons between parametric and non-parametric data, respectively. The test for each experiment is reported in the figure legend.

Acknowledgements

We thank members of the Wolfson Bioimaging facility and Dominic Alibhai for multiphoton microscopy support, Robert Knight for plasmids, Karen Roddy for statistics advice, and members of the Hammond lab for discussions during manuscript preparation.

Competing interests

The authors declare no competing or financial interests.

Author contributions

Conceptualization: L.H.B., E.K., C.L.H.; Methodology: L.H.B., K.B., E.K., S.C., C.L.H.; Software: S.C.; Validation: L.H.B., E.K., C.L.H.; Formal analysis: L.H.B., K.B., E.K., C.L.H.; Investigation: L.H.B., K.B., E.K., C.L.H.; Resources: S.C.; Data curation: L.H.B., K.B., E.K., C.L.H.; Writing - original draft: L.H.B., E.K., S.C., C.L.H.; Writing - review & editing: L.H.B., K.B., E.K., S.C., C.L.H.; Visualization: L.H.B., C.L.H.; Supervision: L.H.B., C.L.H.; Project administration: C.L.H.; Funding acquisition: C.L.H.

Funding

L.H.B. was funded by Wellcome Trust PhD programme 086779/Z/08/A. C.L.H. and E.K. were funded by Arthritis Research UK (19476, 21211). S.C. was funded by the Elizabeth Blackwell Institute, through its Wellcome Trust ISSF Award. Deposited in PMC for immediate release.

Data availability

Raw confocal data are available at at the University of Bristol data repository, data.bris, at https://doi.org/10.5523/bris.3mda1vet7c7wu298pms51n9j1p.

Supplementary information

Supplementary information available online at
http://dev.biologists.org/lookup/doi/10.1242/dev.153528.supplemental

References

Arnsdorf, E. J., Tummala, P. and Jacobs, C. R. (2009). Non-canonical Wnt signaling and N-cadherin related beta-catenin signaling play a role in mechanically induced osteogenic cell fate. *PLoS ONE* **4**, 10.

Askary, A., Smeeton, J., Paul, S., Schindler, S., Braasch, I., Ellis, N. A., Postlethwait, J., Miller, C. T. and Crump, J. G. (2016). Ancient origin of lubricated joints in bony vertebrates. *Elife* **5**, e16415.

Baker-LePain, J. C. and Lane, N. E. (2010). Relationship between joint shape and the development of osteoarthritis. *Curr. Opin. Rheumatol.* **22**, 538-543.

Baker-Lepain, J. C., Lynch, J. A., Parimi, N., McCulloch, C. E., Nevitt, M. C., Corr, M. and Lane, N. E. (2012). Variant alleles of the Wnt antagonist FRZB are determinants of hip shape and modify the relationship between hip shape and osteoarthritis. *Arthritis. Rheum.* **64**, 1457-1465.

Brunt, L. H., Norton, J. L., Bright, J. A., Rayfield, E. J. and Hammond, C. L. (2015). Finite element modelling predicts changes in joint shape and cell behaviour due to loss of muscle strain in jaw development. *J. Biomech.* **48**, 3112-3122.

Brunt, L. H., Roddy, K. A., Rayfield, E. J. and Hammond, C. L. (2016a). Building finite element models to investigate zebrafish jaw biomechanics. *J. Vis. Exp.* doi:10.3791/54811

Brunt, L. H., Skinner, R. E. H., Roddy, K. A., Araujo, N. M., Rayfield, E. J. and Hammond, C. L. (2016b). Differential effects of altered patterns of movement and strain on joint cell behaviour and skeletal morphogenesis. *Osteoarthritis Cartilage* **24**, 1940-1950.

Carrington, B., Varshney, G. K., Burgess, S. M. and Sood, R. (2015). CRISPR-STAT. an easy and reliable PCR-based method to evaluate target-specific sgRNA activity. *Nucleic Acids Res.* **43**, e157.

Chen, J. W. and Galloway, J. L. (2014). The development of zebrafish craniofacial tendon and ligament progenitors. *Am. J. Med. Genet. A* **164**, 1879-1880.

Chen, J. W. and Galloway, J. L. (2017). Using the zebrafish to understand tendon development and repair. *Methods Cell Biol.* **138**, 299-320.

Chen, J. H., Liu, C., You, L. D. and Simmons, C. A. (2010). Boning up on Wolff's Law. Mechanical regulation of the cells that make and maintain bone. *J. Biomech.* **43**, 108-118.

Chen, L.-J., Hu, B.-B., Shi, X.-L., Ren, M.-M., Yu, W.-B., Cen, S.-D., Hu, R.-D. and Deng, H. (2017). Baicalein enhances the osteogenic differentiation of human periodontal ligament cells by activating the Wnt/beta-catenin signaling pathway. *Arch. Oral Biol.* **78**, 100-108.

Church, V., Nohno, T., Linker, C., Marcelle, C. and Francis-West, P. (2002). Wnt regulation of chondrocyte differentiation. *J. Cell Sci.* **115**, 4809-4818.

Clarke, N. M. P. (2014). Swaddling and hip dysplasia. an orthopaedic perspective. *Arch. Dis. Child.* **99**, 5-26.

Clements, W. K., Kim, A. D., Ong, K. G., Moore, J. C., Lawson, N. D. and Traver, D. (2011). A somitic Wnt16/Notch pathway specifies haematopoietic stem cells. *Nature* **474**, 220-224.

Dell'Accio, F., De Bari, C., Eltawil, N. M., Vanhummelen, P. and Pitzalis, C. (2008). Identification of the molecular response of articular cartilage to injury, by microarray screening: Wnt-16 expression and signaling after injury and in osteoarthritis. *Arthritis Rheum.* **58**, 1410-1421.

Dougherty, M., Kamel, G., Grimaldi, M., Gfrerer, L., Shubinets, V., Ethier, R., Hickey, G., Cornell, R. A. and Liao, E. C. (2013). Distinct requirements for wnt9a and irf6 in extension and integration mechanisms during zebrafish palate morphogenesis. *Development* **140**, 76-81.

Edelsbrunner, H., Kirkpatrick, D. G. and Seidel, R. (1983). On the shape of a set of points in the plane. *IEEE Trans. Inf. Theory* **29**, 551-559.

García-Ibarbia, C., Pérez-Núñez, M. I., Olmos, J. M., Valero, C., Pérez-Aguilar, M. D., Hernández, J. L., Zarrabeitia, M. T., González-Macías, J. and Riancho, J. A. (2013). Missense polymorphisms of the WNT16 gene are associated with bone mass, hip geometry and fractures. *Osteoporos. Int.* **24**, 2449-2454.

Gomez, C., David, V., Peet, N. M., Vico, L., Chenu, C., Malaval, L. and Skerry, T. M. (2007). Absence of mechanical loading in utero influences bone mass and architecture but not innervation in Myod-Myf5-deficient mice. *J. Anat.* **210**, 259-271.

Gori, F., Lerner, U., Ohlsson, C. and Baron, R. (2015). A new WNT on the bone. WNT16, cortical bone thickness, porosity and fractures. *Bonekey Rep.* **4**, 669.

Grad, S., Eglin, D., Alini, M. and Stoddart, M. J. (2011). Physical stimulation of chondrogenic cells in vitro. a review. *Clin. Orthop. Relat. Res.* **469**, 2764-2772.

Guo, X. Z., Day, T. F., Jiang, X. Y., Garrett-Beal, L., Topol, L. and Yang, Y. Z. (2004). Wnt/beta-catenin signaling is sufficient and necessary for synovial joint formation. *Genes Dev.* **18**, 2404-2417.

Hammond, C. L. and Schulte-Merker, S. (2009). Two populations of endochondral osteoblasts with differential sensitivity to Hedgehog signalling. *Development* **136**, 3991-4000.

Hartmann, C. and Tabin, C. J. (2000). Dual roles of Wnt signaling during chondrogenesis in the chicken limb. *Development* **127**, 3141-3159.

Hartmann, C. and Tabin, C. J. (2001). Wnt-14 plays a pivotal role in inducing synovial joint formation in the developing appendicular skeleton. *Cell* **104**, 341-351.

Hatta, K., Tsujii, H. and Omura, T. (2006). Cell tracking using a photoconvertible fluorescent protein. *Nat. Protoc.* **1**, 960-967.

Haudenschild, A. K., Hsieh, A. H., Kapila, S. and Lotz, J. C. (2009). Pressure and distortion regulate human mesenchymal stem cell gene expression. *Ann. Biomed. Eng.* **37**, 492-502.

Hruscha, A., Krawitz, P., Rechenberg, A., Heinrich, V., Hecht, J., Haass, C. and Schmid, B. (2013). Efficient CRISPR/Cas9 genome editing with low off-target effects in zebrafish. *Development* **140**, 4982-4987.

Ikegawa, M., Han, H., Okamoto, A., Matsui, R., Tanaka, M., Omi, N., Miyamae, M., Toguchida, J. and Tashiro, K. (2008). Syndactyly and preaxial synpolydactyly in the single Sfrp2 deleted mutant mice. *Dev. Dyn.* **237**, 2506-2517.

Ingber, D. E. (2006). Cellular mechanotransduction: putting all the pieces together again. *FASEB J.* **20**, 811-827.

Jahan, E., Matsumoto, A., Rafiq, A. M., Hashimoto, R., Inoue, T., Udagawa, J., Sekine, J. and Otani, H. (2014). Fetal jaw movement affects Ihh signaling in mandibular condylar cartilage development: the possible role of Ihh as mechanotransduction mediator. *Arch. Oral Biol.* **59**, 1108-1118.

Kahn, J., Shwartz, Y., Blitz, E., Krief, S., Sharir, A., Breitel, D. A., Rattenbach, R., Relaix, F., Maire, P., Rountree, R. B. et al. (2009). Muscle contraction is necessary to maintain joint progenitor cell fate. *Dev. Cell* **16**, 734-743.

Kamel, G., Hoyos, T., Rochard, L., Dougherty, M., Kong, Y., Tse, W., Shubinets, V., Grimaldi, M. and Liao, E. C. (2013). Requirement for frzb and fzd7a in cranial neural crest convergence and extension mechanisms during zebrafish palate and jaw morphogenesis. *Dev. Biol.* **381**, 423-433.

Kobayashi, Y., Thirukonda, G. J., Nakamura, Y., Koide, M., Yamashita, T., Uehara, S., Kato, H., Udagawa, N. and Takahashi, N. (2015). Wnt16 regulates osteoclast differentiation in conjunction with Wnt5a. *Biochem. Biophys. Res. Commun.* **463**, 1278-1283.

Kobayashi, Y., Uehara, S., Udagawa, N. and Takahashi, N. (2016). Regulation of bone metabolism by Wnt signals. *J. Biochem.* **159**, 387-392.

Lee, R. T. H., Knapik, E. W., Thiery, J. P. and Carney, T. J. (2013). An exclusively mesodermal origin of fin mesenchyme demonstrates that zebrafish trunk neural crest does not generate ectomesenchyme. *Development* **140**, 2923-2932.
Li, Y. and Dudley, A. T. (2009). Noncanonical frizzled signaling regulates cell polarity of growth plate chondrocytes. *Development* **136**, 1083-1092.
Li, J., Duncan, R. L., Burr, D. B. and Turner, C. H. (2002). L-type calcium channels mediate mechanically induced bone formation in vivo: *J. Bone Miner. Res.* **17**, 1795-1800.
Luterkort, M., Persson, P. H., Polberger, S. and Bjerre, I. (1986). Hip-joint instability in breech pregnancy. *Acta Paediatrica Scandinavica* **75**, 860-863.
Mavčič, B., Iglič, A., Kralj-Iglič, V., Brand, R. A. and Vengust, R. (2008). Cumulative hip contact stress predicts osteoarthritis in DDH. *Clin. Orthop. Relat. Res.* **466**, 884-891.
Moreno-Mateos, M. A., Vejnar, C. E., Beaudoin, J. D., Fernandez, J. P., Mis, E. K., Khokha, M. K. and Giraldez, A. J. (2015). CRISPRscan. designing highly efficient sgRNAs for CRISPR-Cas9 targeting in vivo. *Nat. Methods* **12**, 982-988.
Moro, E., Ozhan-Kizil, G., Mongera, A., Beis, D., Wierzbicki, C., Young, R. M., Bournele, D., Domenichini, A., Valdivia, L. E., Lum, L. et al. (2012). In vivo Wnt signaling tracing through a transgenic biosensor fish reveals novel activity domains. *Dev. Biol.* **366**, 327-340.
Murray, P. D. F. and Selby, D. (1930). Intrinsic and extrinsic factors in the primary development of the skeleton. *Wilhelm Roux Archiv Fur Entwicklungsmechanik Der Organismen* **122**, 629-662.
Mutoh, T., Miyata, T., Kashiwagi, S., Miyawaki, A. and Ogawa, M. (2006). Dynamic behavior of individual cells in developing organotypic brain slices revealed by the photoconvertable protein Kaede. *Exp. Neurol.* **200**, 430-437.
Nayak, S. S., Kadavigere, R., Mathew, M., Kumar, P., Hall, J. G. and Girisha, K. M. (2014). Fetal akinesia deformation sequence: expanding the phenotypic spectrum. *Am. J. Med. Genet. A* **164A**, 2643-2648.
Niehrs, C. (2012). The complex world of WNT receptor signalling. *Nat. Rev. Mol. Cell Biol.* **13**, 767-779.
Nowlan, N. C., Prendergast, P. J. and Murphy, P. (2008). Identification of mechanosensitive genes during embryonic bone formation. *PLoS Comput. Biol.* **4**, 10.
Nowlan, N. C., Bourdon, C., Dumas, G., Tajbakhsh, S., Prendergast, P. J. and Murphy, P. (2010a). Developing bones are differentially affected by compromised skeletal muscle formation. *Bone* **46**, 1275-1285.
Nowlan, N. C., Sharpe, J., Roddy, K. A., Prendergast, P. J. and Murphy, P. (2010b). Mechanobiology of embryonic skeletal development. insights from animal models. *Birth Defects Res. C Embryo Today* **90**, 203-213.
Otsu, N. (1979). A threshold selection method from gray-level histograms. *IEEE Trans. Syst. Man Cybern.* **9**, 62-66.
Ozeki, N., Mogi, M., Hase, N., Hiyama, T., Yamaguchi, H., Kawai, R., Kondo, A. and Nakata, K. (2016). Wnt16 signaling is required for IL-1 beta-induced matrix metalloproteinase-13-regulated proliferation of human stem cell-derived osteoblastic cells. *Int. J. Mol. Sci.* **17**, 221.
Pacifici, M., Koyama, E., Shibukawa, Y., Wu, C. S., Tamamura, Y., Enomoto-Iwamoto, M. and Iwamoto, M. (2006). Cellular and molecular mechanisms of synovial joint and articular cartilage formation. *Ann. N Y Acad Sci.* **1068**, 74-86.
Pan, Y. A., Freundlich, T., Weissman, T. A., Schoppik, D., Wang, X. C., Zimmerman, S., Ciruna, B., Sanes, J. R., Lichtman, J. W. and Schier, A. F. (2013). Zebrabow. multispectral cell labeling for cell tracing and lineage analysis in zebrafish. *Development* **140**, 2835-2846.
Pazin, D. E., Gamer, L. W., Cox, K. A. and Rosen, V. (2012). Molecular profiling of synovial joints: use of microarray analysis to identify factors that direct the development of the knee and elbow. *Dev. Dyn.* **241**, 1816-1826.
Rochard, L., Monica, S. D., Ling, I. T. C., Kong, Y., Roberson, S., Harland, R., Halpern, M. and Liao, E. C. (2016). Roles of Wnt pathway genes wls, wnt9a, wnt5b, frzb and gpc4 in regulating convergent-extension during zebrafish palate morphogenesis. *Development* **143**, 2541-2547.
Roddy, K. A., Nowlan, N. C., Prendergast, P. J. and Murphy, P. (2009). 3D representation of the developing chick knee joint. a novel approach integrating multiple components. *J. Anat.* **214**, 374-387.
Roddy, K. A., Prendergast, P. J. and Murphy, P. (2011). Mechanical influences on morphogenesis of the knee joint revealed through morphological, molecular and computational analysis of immobilised embryos. *PLoS ONE* **6**, e17526.
Rodrigues, F., Doughton, G., Yang, B. J. and Kelsh, R. N. (2012). A novel transgenic line using the Cre-lox system to allow permanent lineage-labeling of the zebrafish neural crest. *Genesis* **50**, 750-757.
Rolfe, R., Roddy, K. and Murphy, P. (2013). Mechanical regulation of skeletal development. *Curr. Osteoporos Rep.* **11**, 107-116.
Rolfe, R. A., Nowlan, N. C., Kenny, E. M., Cormican, P., Morris, D. W., Prendergast, P. J., Kelly, D. and Murphy, P. (2014). Identification of mechanosensitive genes during skeletal development: alteration of genes associated with cytoskeletal rearrangement and cell signalling pathways. *BMC Genomics* **15**, 48.
Rotherham, M. and El Haj, A. J. (2015). Remote activation of the Wnt/beta-catenin signalling pathway using functionalised magnetic particles: *PLoS ONE*, **10**, e0121761.
Rot-Nikcevic, I., Reddy, T., Downing, K. J., Belliveau, A. C., Hallgrimsson, B., Hall, B. K. and Kablar, B. (2006). Myf5(-/-). MyoD(-/-) amyogenic fetuses reveal the importance of early contraction and static loading by striated muscle in mouse skeletogenesis. *Dev. Genes Evol.* **216**, 1-9.
Rot-Nikcevic, I., Downing, K. J., Hall, B. K. and Kablar, B. (2007). Development of the mouse mandibles and clavicles in the absence of skeletal myogenesis. *Histol. Histopathol.* **22**, 51-60.
Schindelin, J., Arganda-Carreras, I., Frise, E., Kaynig, V., Longair, M., Pietzsch, T., Preibisch, S., Rueden, C., Saalfeld, S., Schmid, B. et al. (2012). Fiji: an open-source platform for biological-image analysis. *Nat. Methods* **9**, 676-682.
Shea, C. A., Rolfe, R. A. and Murphy, P. (2015). The importance of foetal movement for co-ordinated cartilage and bone development in utero: clinical consequences and potential for therapy. *Bone Joint Res.* **4**, 105-116.
Shwartz, Y., Farkas, Z., Stern, T., Aszódi, A. and Zelzer, E. (2012). Muscle contraction controls skeletal morphogenesis through regulation of chondrocyte convergent extension. *Dev. Biol.* **370**, 154-163.
Shwartz, Y., Viukov, S., Krief, S. and Zelzer, E. (2016). Joint development involves a continuous influx of Gdf5-positive cells. *Cell Rep.* **15**, 2577-2587.
Sugano, N., Noble, P. C., Kamaric, E., Salama, J. K., Ochi, T. and Tullos, H. S. (1998). The morphology of the femur in developmental dysplasia of the hip. *J. Bone Joint Surg. Br.* **80**, 711-719.
Teh, M.-T., Blaydon, D., Ghali, L. R., Briggs, V., Edmunds, S., Pantazi, E., Barnes, M. R., Leigh, I. M., Kelsell, D. P. and Philpott, M. P. (2007). Role for WNT16B in human epidermal keratinocyte proliferation and differentiation (vol 120, pg 330, 2007). *J. Cell Sci.* **120**, 917-917.
Thisse, C. and Thisse, B. (2008). High-resolution in situ hybridization to whole-mount zebrafish embryos. *Nat. Protoc.* **3**, 59-69.
van den Bosch, M. H., Blom, A. B., Sloetjes, A. W., Koenders, M. I., van de Loo, F. A., van den Berg, W. B., van Lent, P. L. and van der Kraan, P. M. (2015). Induction of canonical Wnt signaling by synovial overexpression of selected Wnts leads to protease activity and early osteoarthritis-like cartilage damage. *Am. J. Pathol.*, **185**, 1970-1980.
Wergedal, J. E., Kesavan, C., Brommage, R., Das, S. and Mohan, S. (2015). Role of WNT16 in the regulation of periosteal bone formation in female mice. *Endocrinology* **156**, 1023-1032.
Westerfield, M. (2000). *The Zebrafish Book. A Guide for the Laboratory Use of Zebrafish (danio rerio)*. University of Oregon, OR: University of Oregon Press.
Willert, K. and Nusse, R. (2012). Wnt proteins. *Cold Spring Harb. Perspect. Biol.* **4**, a007864.
Witte, F., Dokas, J., Neuendorf, F., Mundlos, S. and Stricker, S. (2009). Comprehensive expression analysis of all Wnt genes and their major secreted antagonists during mouse limb development and cartilage differentiation. *Gene Expr. Patterns* **9**, 215-223.
Yang, Y., Topol, L., Lee, H. and Wu, J. (2003). Wnt5a and Wnt5b exhibit distinct activities in coordinating chondrocyte proliferation and differentiation. *Development* **130**, 1003-1015.
Zhang, L., Liu, W., Zhao, J., Ma, X., Shen, L., Zhang, Y., Jin, F. and Jin, Y. (2016). Mechanical stress regulates osteogenic differentiation and RANKL/OPG ratio in periodontal ligament stem cells by the Wnt/beta-catenin pathway. *Biochim. Biophys. Acta* **1860**, 2211-2219.